ACS APPLIED MATERIALS & INTERFACES

Research Article

www.acsami.org

A Facile and Green Approach for the Controlled Synthesis of Porous SnO_2 Nanospheres: Application as an Efficient Photocatalyst and an Excellent Gas Sensing Material

P. Manjula, Ramireddy Boppella, and Sunkara V. Manorama*

Nanomaterials Laboratory, Inorganic & Physical Chemistry Division, Indian Institute of Chemical Technology, Hyderabad -500 007, Andhra Pradesh, India

Supporting Information

ABSTRACT: A facile and elegant methodology invoking the principles of Green Chemistry for the synthesis of porous tin dioxide nanospheres has been described. The low-temperature (~50 °C) synthesis of SnO_2 nanoparticles and their self-assembly into organized, uniform, and monodispersed porous nanospheres with high surface area is facilitated by controlling the concentration of glucose, which acts as a stabilizing as well as structure-directing agent. A systematic control on the stannate to glucose molar concentration ratio determines the exact conditions to obtain monodispersed nanospheres, preferentially over random aggregation. Detailed characterization of the structure, morphology, and chemical composition reveals that the synthesized material, 50 nm SnO_2 porous nanospheres possess BET surface area of about 160 m^2/g. Each porous nanosphere consists of a few hundred nanoparticles ~2−3 nm in diameter with tetragonal cassiterite crystal structure. The SnO_2 nanospheres exhibit elevated photocatalytic activity toward methyl orange with good recyclability. Because of the high activity and stability of this photocatalyst, the material is ideal for applications in environmental remediation. Moreover, SnO_2 nanospheres display excellent gas sensing capabilities toward hydrogen. Surface modification of the nanospheres with Pd transforms this sensing material into a highly sensitive and selective room-temperature hydrogen sensor.

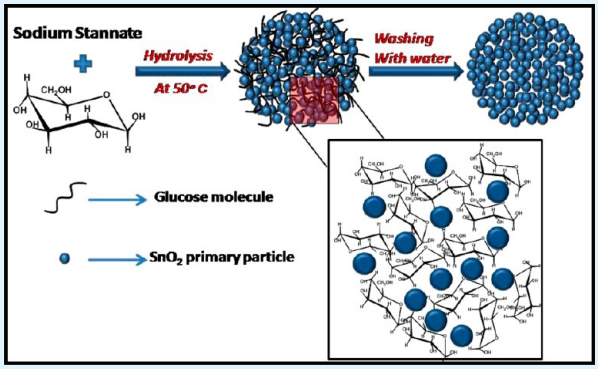

KEYWORDS: *SnO_2, porous nanospheres, low-temperature synthesis, self-assembly, photocatalysis, hydrogen gas sensing*

1. INTRODUCTION

Current research activity in Materials Chemistry and Physics is directed toward efficient "Green Technologies" primarily driven by environmental concerns and economic issues leading to the development of low-temperature, cost-effective, and easily upscalable strategies for materials synthesis. It is now accepted beyond doubt that nanostructuring adds value to material properties and diversifies the application areas. This has led to intense activity being witnessed globally, aimed at developing new methods to synthesize nanostructured materials with desired morphologies, albeit with novel structural features and improved physical, chemical, and electronic properties. Added to this, an ability to self-assemble the nanosized material[1] makes these materials versatile for a large number of specialized applications.[2−5]

Glucose, a well-known capping and reducing agent, has been used extensively in the synthesis of hierarchical nanostructured metals and metal oxides with controlled morphology and porosity.[6−8] Over the years, several strategies have been perfected to obtain porous materials with large specific surface area.[9,10] Because of their remarkably high surface area, porosity, and unique adsorption property, these porous materials are ideal building blocks for the construction of a range of devices like carriers in drug delivery,[11] in lithium ion batteries,[12] as electrodes in dye-sensitized solar cells (DSSCs)[13] and as gas sensors.[14,15] In spite of all these efforts, there is still a primary challenge to explore newer methodologies that would simplify the synthesis process to obtain the materials with suitable morphologies, that are cost-effective and easily upscalable. In particular, synthesis of wide band gap semiconducting oxide materials ZnO, SnO_2, TiO_2, etc. have gained special attention for the above applications owing to their sensitivity to surface charge and wide temperature stability. Among them tin dioxide is one of the most well-known and extensively studied material owing to its several interesting properties that makes it ideal for a wide range of applications.[16−20] Stoichiometric tin oxide is an insulator but the technologically more important properties of this material arise from the non stoichiometric nature of the oxide that imparts it semiconducting properties.[21] Control of its oxidation state renders it unique physical and electronic

Received: August 31, 2012
Accepted: October 22, 2012
Published: October 22, 2012

   dx.doi.org/10.1021/am301840s | ACS Appl. Mater. Interfaces 2012, 4, 6252−6260

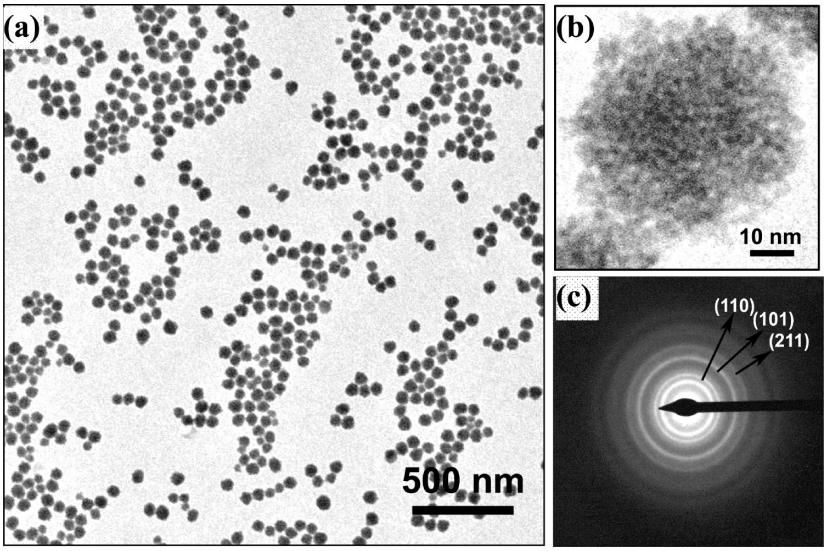

Figure 1. (a) TEM micrograph of as-synthesized porous SnO_2 nanospheres. (b) High-magnification TEM micrograph of SnO_2 nanosphere. (c) SAED pattern of SnO_2 nanospheres from Philips Technai G2 FEI F12 transmission electron microscope operating at 80−100 kV by dispersing samples in ethanol and loaded on Formvar-coated copper grids.

properties suitable for applications in sensing,[22,23] as conducting coatings,[24] in photocatalysis,[5] and for battery applications[25,26] as well.

This paper demonstrates a facile, viable, eco-friendly, and economical route for the large scale synthesis of porous SnO_2 nanospheres via a modified hydrolysis route. We report a novel approach for the preparation of porous nanospheres comprising ultrasmall SnO_2 nanoparticles. The chemically induced self-assembly of SnO_2 nanoparticles (∼2−3 nm) into nanospheres (∼50 nm) by using glucose as the structure directing agent makes the entire synthesis convenient and green. The synthesis method adopted offers the following advantages: (1) it avoids use of noxious or perilous chemicals and organic solvents during the entire reaction procedure, (2) it is a low temperature synthesis, (3) the reasonably low cost of chemical precursors makes it economical, and (4) it is convenient for up scaling.

Photocatalysis and gas sensing based on SnO_2 in particular could be conveniently and effectively engineered by controlling the size, morphology, surface to volume ratio, porosity, and surface active sites. As a photocatalyst for the degradation of pollutants, it is very important that the material being used should not by itself contribute to pollution. Due to photo erosion many binary compounds for example, ZnO and many sulfides can cause secondary pollution which restricts their applicability. Along with TiO_2, SnO_2 is an ideal material for photocatalytic applications because of its high stability and alkali and acid resistance.

To the best of our knowledge, the procedure reported in this paper and the product obtained is probably the first report on the synthesis of porous SnO_2 nanospheres at low temperature starting with stannate precursor and glucose as structure modifying agent. The advantages offered by the material synthesized has been exploited in terms of efficient photocatalytic properties and excellent gas sensing capabilities viz. lower operating temperature, sensitivity to lower gas concentration, and faster response rate. Surface decoration with Pd makes it a superior sensor for the selective detection of hydrogen with a high figure of merit.

2. EXPERIMENTAL SECTION

2.1. Synthesis of SnO_2 Nanospheres. In a typical procedure for synthesizing porous SnO_2 nanospheres, 1 g of sodium stannate trihydrate (Alfa Aesar) is dissolved in 30 mL of deionized water (18.2 MΩ) to get 0.125 M stannate solution in a round-bottom flask and 2 g of D-glucose monohydrate (Sigma Aldrich) was added to the freshly prepared stannate solution and kept for stirring at 50 °C. After 12 h of reaction the formed white precipitate was collected by centrifugation and washed with deionized water and kept for drying at 50 °C. Thorough experimentation has been carried out by varying time and glucose concentrations to study their effect on the size and morphology of the product.

2.2. Incorporation of Pd Nanoparticles into SnO_2 Nanospheres. To synthesize 0.5 wt % Pd/SnO_2, we dispersed the synthesized 0.5 g of SnO_2 nanospheres and 6.9 mg of sodium tetra chloro palladate (Sigma Aldrich) in 40 mL of deionized water (18.2 MΩ). This was followed by the addition of sodium borohydride to reduce the palladium salt to metallic Pd. This procedure resulted in 0.5 wt % Pd nanoparticles embedded on the SnO_2 nanospheres. The resulting Pd/SnO_2 product was centrifuged and washed thoroughly with deionized water and dried at 50 °C.

2.3. Photodegradation Experiment. In a typical reaction, 0.03 g of SnO_2 nanospheres was dispersed in 30 mL of aqueous methyl orange (MO) (2.5×10^{-5} M)) in a quartz reactor. Prior to irradiation, the suspension was magnetically stirred for 30 min in dark to stabilize and equilibrate the adsorption of MO on the surface of porous SnO_2 nanospheres. The stable aqueous MO-SnO_2 suspension was then exposed to UV light irradiation under continual stirring. Five ml aliquots were withdrawn at regular time intervals to carry out the constituent analysis. The concentration of MO (C/C_0) was estimated using UV−vis spectroscopy after separating the SnO_2 catalyst sample from the mixture.

2.4. Gas Sensing Experiment. For the gas sensing measurements, the synthesized SnO_2 nanospheres were mixed with deionized water to form a paste and brush coated onto cylindrical alumina tubes of length 15 mm and diameter 5 mm already provided with two Pt wire electrodes for the electrical contacts. A heating coil was inserted inside the alumina tube to maintain the desired temperature during gas sensing and the temperature measured using a Chromel-Alumel K type thermo couple in contact with the sensor surface. The sensor surface was stabilized by heating the sensor element at 150 °C for 2 h in air.[14]

3. RESULTS AND DISCUSSION

Figure 1a is a representative TEM image of the as synthesized product showing reasonably monodispersed nanospheres with average size around 50 ± 5 nm. The high-magnification TEM image (Figure 1b) reveals that each nanosphere comprises of few hundred primary nanoparticles with a size of about 2−3 nm. Figure 1c is the selected area electron diffraction (SAED) pattern with the major characteristic diffraction rings of SnO_2. The FESEM micrograph (Figure.2) reveals the rough surface morphology of the nanospheres recorded on a Carl Zeiss model ultra 55 FESEM.

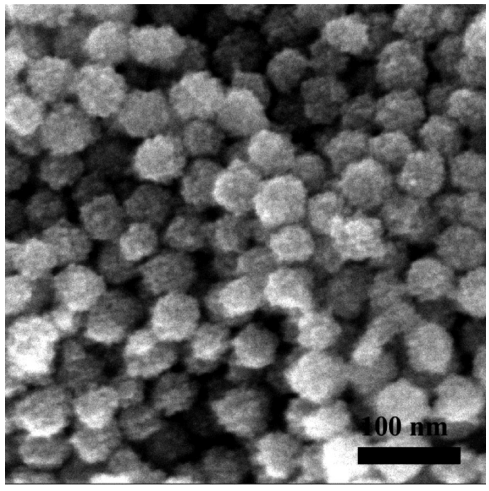

Figure 2. FESEM image of as synthesized porous SnO_2 nanospheres recorded on a Carl Zeiss model ultra 55 FESEM.

Selected area electron diffraction (SAED) pattern (Figure.1c) and X-ray diffraction studies in Figure 3 confirmed that the

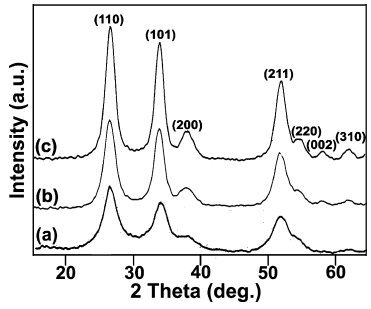

Figure 3. X-ray diffraction patterns of porous SnO_2 nanospheres (a) as-synthesized, (b) calcined at 300 °C, and (c) calcined at 500 °C temperatures from Siemens (Cheshire, U.K.) D5000 X-ray diffractometer over a 2θ range of 2−65° using Cu Kα radiation (1.5406 Å) at 40 kV and 30 mA with a standard monochromator using a Ni filter.

synthesized materials are SnO_2 of tetragonal cassiterite structure. The diffraction peaks indexed from the XRD studies matched the reported JCPDS data (Card No: 21−1250). Slight broadening of the peaks is expected because of smaller crystallite size of the particles.[14]

The crystallite size calculated by applying the Scherrer's formula to the major diffraction peaks in the XRD pattern is about 2.9 nm for the as synthesized SnO_2 nanospheres and 3.2, 4.6, and 5.9 nm for SnO_2 samples calcined at 150, 300, and 500 °C, respectively. The crystallite size of SnO_2 samples calcined at different temperatures is in good agreement with primary particle size of SnO_2 samples from TEM micrographs (see Figure S-1 in the Supporting Information). These TEM micrographs reveal that, on calcination the primary particles tend to agglomerate and increase the constituent particle size within the sphere but the overall size of SnO_2 nanospheres remains unchanged. The size of the primary particles in the as synthesized SnO_2 nanospheres and in the calcined nanospheres at 150, 300, and 500 °C are about ∼2−3, ∼3−4, ∼5−6, and ∼7−8 nm, respectively. This increase in the size of the SnO_2 primary particles is due to the classical crystallization process well-known as Ostwald ripening.

The size distribution of SnO_2 nanospheres as obtained from the DLS studies in Figure 4 estimates the average hydro-

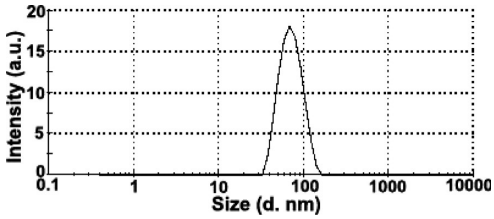

Figure 4. DLS of as synthesized porous SnO_2 nanospheres on a Zetasizer 3000HSA (Malvern instruments, UK) using a 90° scattering angle and a laser light of wavelength 633 nm. The hydrodynamic diameter of particles was calculated by using the automated mode. The system was calibrated using the 199 ± 6 nm Nanospheres Size Standard (Duke Scientific Corp., Palo Alto, CA, USA) and DTS 0050 standard from Malvern.

dynamic diameter of SnO_2 nanospheres to be about 67 nm. It is clearly evident that nanospheres are uniform and monodispersed and the mean size distribution is in good agreement with TEM micrographs. The Brunauer−Emmett−Teller (BET) surface area measurements give a specific surface area value of about 160 $m^2\ g^{-1}$ for the as synthesized porous SnO_2 nanospheres degassed at 100 °C. The samples calcined at 150, 200, 300, and 500 °C possess surface areas of 147, 130, 103, and 75 $m^2\ g^{-1}$, respectively. All these characterizations establish that the synthesized product is pure SnO_2 with high specific surface area. The typical nitrogen adsorption−desorption isotherm and BJH pore size distribution gives a value of 2.55 nm for the average pore size and a pore volume of 0.196 cc/g for the SnO_2 nanospheres from Figure 5.

TG and DTA (see Figure S-2 in the Supporting Information) of SnO_2 nanospheres in the range from room temperature to

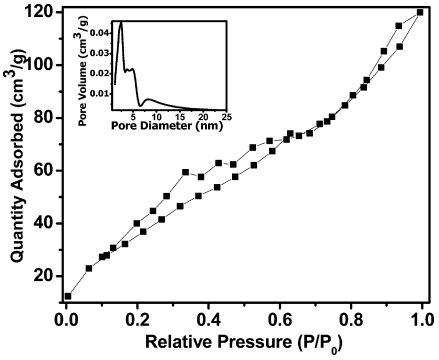

Figure 5. Typical N_2 sorption isotherm and the corresponding Barrett−Joyner−Halenda (BJH) pore size distribution plot (inset) of the porous SnO_2 nanospheres.

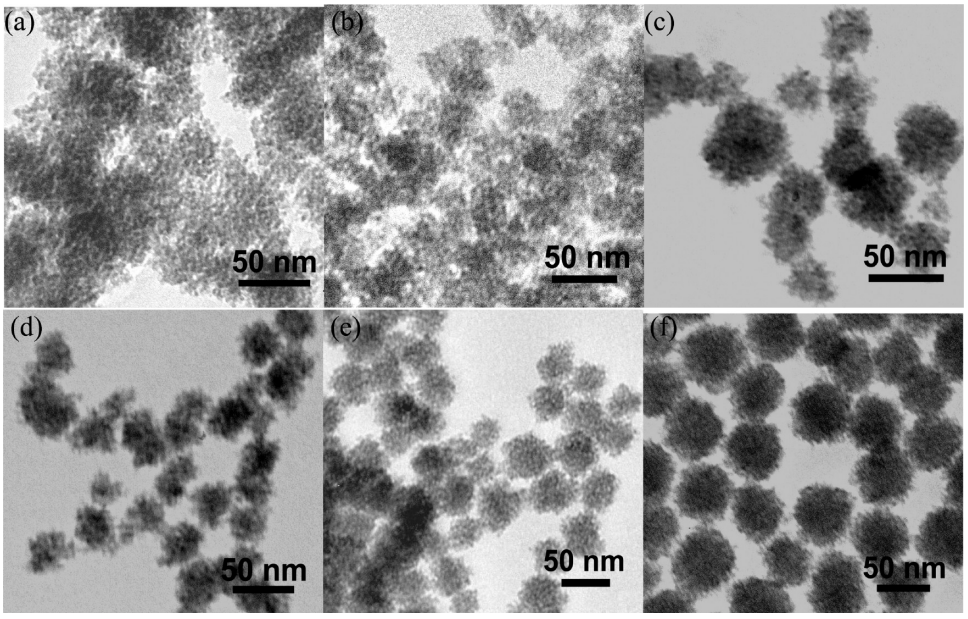

Figure 6. Series of TEM micrographs showing the gradual transformation of irregularly shaped nanoclusters to well-defined nanospheres by self-assembly method by varying the stannate to glucose molar ratio for the reaction time 12 h: (a) no glucose, (b) 1:0.25, (c) 1:0.5, (d) 1:1, (e) 1:2, (f) 1:2.5.

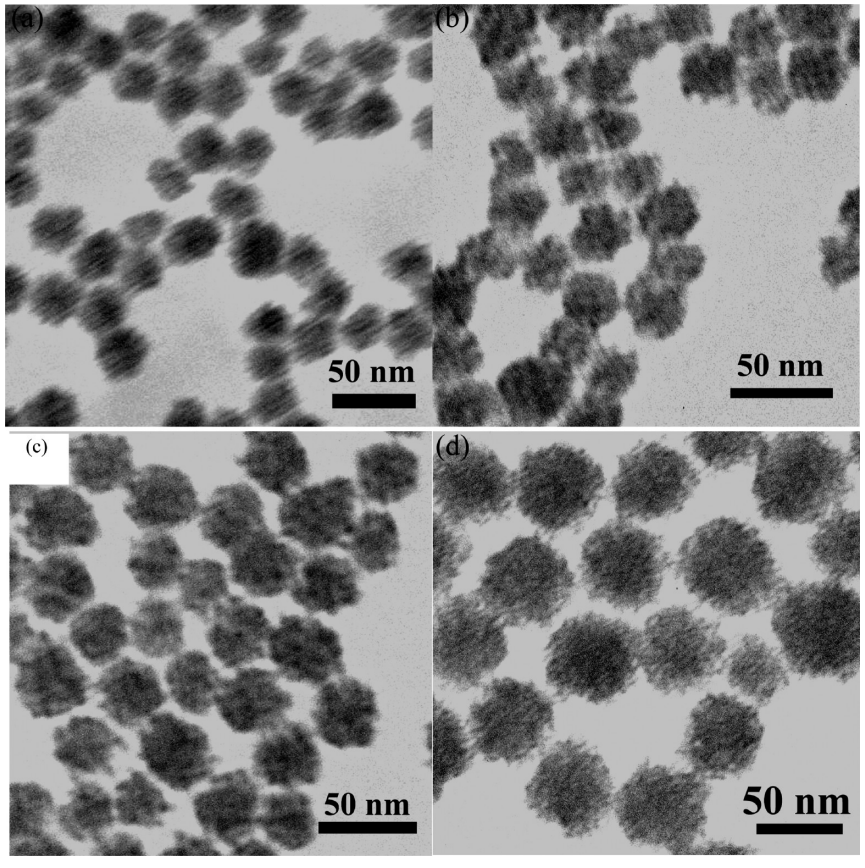

Figure 7. TEM micrographs of SnO_2 nanospheres at different reaction times at 50 °C and the stannate to glucose molar ratio 1:2.5: (a) 1, (b) 3, (c) 6, and (d) 12 h.

1000 °C reveals the stability of SnO_2 assemblies. The first strong weight loss peak around 110 °C is due to the removal of surface adsorbed water which corresponds to the endothermic peak at the same temperature in DTA spectra. The second obvious weight loss in the 200−500 °C region is assigned to the desorption of O^- and O^{2-} and could be attributed to the dehydration process corresponding to the conversion of tin hydroxide to tin oxide as well as progressive crystallization,[21] and also charring of residual glucose. During this process there is a weight loss of about 8%. The stability of the material is

dx.doi.org/10.1021/am301840s | ACS Appl. Mater. Interfaces 2012, 4, 6252−6260

Scheme 1. Schematic Representation Illustrating the Synthesis Mechanism of Porous SnO_2 Nanospheres

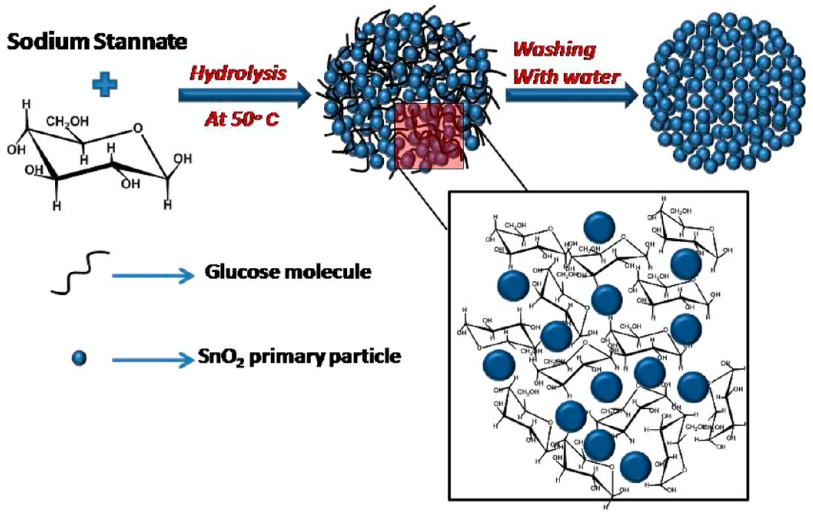

confirmed from the TG-DTA curve which shows no weight loss above 500 °C. FT-IR spectrum (see Figure S-3 in the Supporting Information) of porous SnO_2 nanospheres shows the peak at 3420 cm^{-1} due to the stretching vibration of OH groups[27] and the peak at 1641 cm^{-1} attributed to the bending vibration of the adsorbed molecular water and the small hump at 970 cm^{-1} assigned to surface oxygen (Sn−O_{surf}).[28] Broad and intense vibration at 750−400 cm^{-1} can be assigned to the Sn−O lattice vibration of SnO_2.[29] Energy dispersive X-ray scattering (EDX) (see Figure S-4 in the Supporting Information) confirmed the presence of O, Pd, and Sn elements in the sample, and Table S-1 in the Supporting Information gives the details of the composition from EDX analysis and confirms the presence of Pd (0.14 wt %) in the SnO_2 matrix.

4. REACTION MECHANISM

To understand the role of each of the parameters on the growth process of the SnO_2 nanospheres, a series of experiments were devised by varying the stannate to glucose molar ratio and the reaction time.

4.1. Effect of Molar Ratio. Figure 6 is a series of TEM micrographs that reveal the gradual transformation of dispersed nanoparticles to irregularly shaped nanoclusters and finally into well-defined spherical nanospheres by self-assembly, depending on the glucose concentration. When the reaction was carried out in the absence of glucose, irregular aggregation of nanoparticles was observed because of the rapid and uncontrolled aggregation of primary nanoparticles. This definitely suggests that glucose does play a role in the formation of spherical aggregates. To assign the role of glucose in the reaction procedure, we monitored the self-assembling process of porous SnO_2 nanospheres by systematically varying the stannate to glucose molar ratio from 1:0 (blank reaction) to 1: 2.5 (1:0, 1:0.25, 1:0.5, 1:1, 1:2, 1:2.5) and observed the corresponding TEM micrographs. Well-formed porous nanospheres of about 50 nm comprising of ultrasmall individual particles are obtained as observed in Figure 6f at a stannate to glucose molar ratio of 1:2.5. From this study it can be inferred that the role of glucose is to inhibit the spontaneous aggregation and promote the controlled self-assembly of the SnO_2 nanoparticles into well-formed nanospheres as elaborated below.

In the initial stages, a simple hydrolysis of sodium stannate results in numerous primary SnO_2 nanocrystals in solution which are immediately entrapped by glucose molecules (capping agent). This protection controls the aggregation in such a way as to form well-defined nanospheres subsequently and prevent random and spontaneous aggregation. The probable driving force behind this mechanism is attainment of minimal surface energy of the assembly by forming spheres, supported by strong hydrogen bonding between the glucose molecules adsorbed on the SnO_2 nanoparticles.[30] This attribute was adequately evident in the present study, where we discovered that the glucose concentration played a key role in controlling the morphology and size of the SnO_2 nanoarchitectures. Glucose thus facilitates the stabilizing process by entrapping SnO_2 nanocrystals favoring controlled aggregation.

4.2. Effect of Reaction Time. Time-dependent morphology progression of SnO_2 nanospheres was also investigated using TEM. It is evident from Figure 7 that the reaction time plays a significant role in forming well-defined, uniform SnO_2 nanospheres. Figure 7 clearly illustrates the changes in size of SnO_2 nanospheres obtained from the material synthesized with different reaction times. One hour reaction time leads to aggregation of primary particles forming small aggregates of nanospheres that are not well formed and the yield is also very low. On increasing the reaction time, SnO_2 nanospheres gradually transform from random, small aggregates to well-defined, regular and bigger sized nanospheres. As the reaction progresses the yield improves and the nanospheres subsequently becoming regular, well-formed, and at the end of 12 h, attain a diameter of ∼50 nm.

From the above studies, the following could be the probable reaction pathway that could explain the formation of porous SnO_2 nanospheres under the described conditions. In the initial stages of the reaction synthesis low temperature hydrolysis of sodium stannate leads to formation of nanocrystallites by slow nucleation. Once the nanocrystallites are formed in the solution, glucose gets spontaneously adsorbed on it and acts as a soft template to direct the growth of SnO_2 nanospheres. Driven by hydrogen bonding between glucose molecules, the primary nanocrystallites form nanoaggregates by self-assembly

method that can be described as imperfect oriented attachment mechanism.[30,31] In this mechanism, the primary nanocrystallites possess high surface energies and have a stronger tendency to aggregate into nanospheres by lattice fusion of the adjacent crystallographic planes. Because there is no specific crystal plane orientation, anisotropic unidirectional crystal growth is not favored. In this process glucose acts as a capping agent to prevent random aggregation. Because smaller spheres with larger curvature possess higher surface energies, and thus increased tendency to aggregate with nanocrystallites the process continues until the nanospheres are stabilized by their surface energy.[30] The evolution of nanospheres by self-assembly of the SnO_2 nanoparticles can be postulated as a schematic illustration displayed in Scheme 1.

5. APPLICATIONS

The synthesized and well-characterized porous SnO_2 nanospheres are suitable for a wide variety of applications. In the present study we focus on two applications which are significant because of their great impact on energy and environment viz. photocatalytic degradation of pollutants and gas sensing.

5.1. Photochemical Studies. The photocatalytic performance of porous SnO_2 nanospheres was demonstrated by room temperature UV-light degradation of methyl orange, a very common textile industry pollutant dye in water. The degradation of MO was monitored by observing the characteristic absorption peak at about 457 nm and the gradual decrease in intensity on irradiation with a 400 W UV light source (360 nm, High pressure Hg vapor lamp, SAIC, India) which was used as the light source in an indigenously fabricated photochemical reactor, with a cylindrical glass jacket for water circulation around the lamp. The reactor temperature is maintained by circulating cold water.

It is well-known that the morphology, porosity, surface area, and crystallinity of the material are some of the factors that play a key role in the performance of a material as a photocatalyst.[32] Increased crystallinity with increase in calcination temperature definitely favors photocatalytic activity, but the decrease in surface area is detrimental to the photocatalytic activity. Hence, an optimum temperature has to be reached for the best performance. Toward this end, detailed studies were carried out to understand the effect of crystallinity and surface area of SnO_2 nanospheres on the photocatalytic activity. Figure 8 presents the UV−visible absorption spectra of the aqueous methyl orange solution using SnO_2 nanospheres calcined at 150 °C, exposed to 400 W UV light for various durations. It is seen from Figure 8 that using SnO_2 nanospheres calcined at 150 °C the MO aqueous solution was completely degraded in 30 min. Figure 9 shows the photodegradation curves of methyl orange solution using SnO_2 nanospheres calcined at different temperatures as catalysts under irradiation with UV light. The as synthesized SnO_2 nanospheres (S-A) showed 84% degradation in 30 min and the samples calcined at 150 °C (S-150), 200 °C (S-200), 300 °C (S-300), and 500 °C (S-500) degraded MO to the extent of approximately 100, 87, 62, and 42%, respectively, in 30 min. These observations suggest that the sample S-150 with moderate surface area (146 $m^2\ g^{-1}$) and crystallinity is the best photocatalyst for the reaction under study among the studied materials. The table summarizes the results of the photocatalytic studies and the physical characterisctics of the material used as the photocatalyst. In addition to these parameters, the porosity offered by the assembled SnO_2 nanospheres is also a contributing factor in improving the photocatalytic efficiency. Porous materials offer more accessibility for the dye to contact the material directly, that enhances the photocatalytic reaction and thereby the photocatalytic degradation of the pollutant dye.

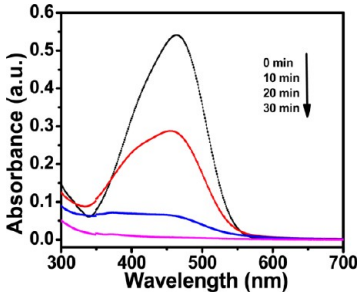

Figure 8. UV−visible spectroscopic changes of the aqueous methyl orange solution in the presence of the SnO_2 nanospheres calcined at 150 °C under UV irradiation.

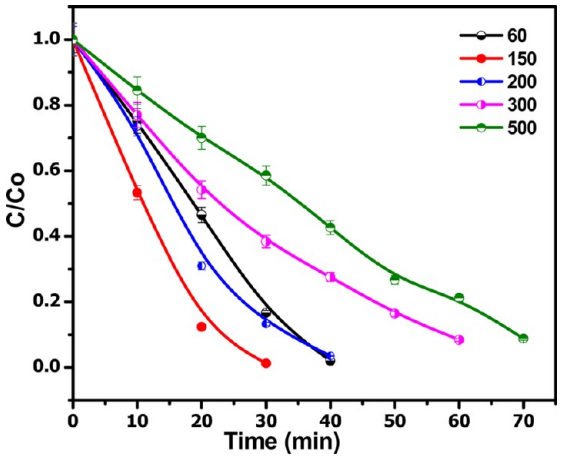

Figure 9. Photodegradation curves of methyl orange solution by using the SnO_2 nanospheres calcined at different temperatures as catalysts under irradiation with UV light.

To assess the recyclability performance of SnO_2 nanospheres, which is also an important criterion for the applicability of the materials for photocatalysis, we carried out five cycles of photocatalytic degradation of MO using the S-150 sample. Figure 10 is the photocatalytic efficiency of S-150; there is no noticeable change within the 5 cycles. This implies that the material does not undergo any degradation during the reaction.

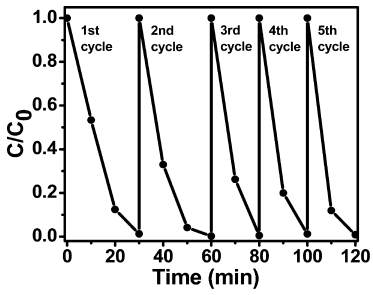

Figure 10. Five cycles of the photocatalytic degradation of MO in the presence of the SnO_2 nanospheres calcined at 150 °C under the UV−vis light irradiation.

This fact is reiterated by the XRD data (Figure 11), which shows no change in the diffraction pattern before and after the

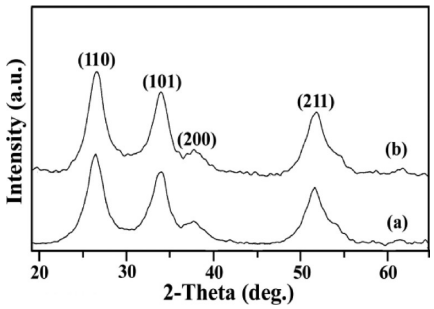

Figure 11. X-ray diffraction patterns of SnO_2 nanospheres (a) before and (b) after photocatalysis.

photocatalytic reaction. As an additional benefit we found that the preformed assembly of SnO_2 nanoparticles aid in easy separation of the catalyst from the reaction solution. The catalyst separation from the material mixture was possible by a simple 5 min centrifugation at a speed of 5000 rpm. From XRD and TEM results (see Figure S-10 in the Supporting Information), there is no evident change in structure and morphology after the photocatalysis reaction. All these results unambiguously conclude that the SnO_2 nanospheres are morphologically stable in the process of the photocatalytic reaction.

Table 1. Photocatalytic Degradation Percentage of Methyl Orange by SnO_2 Nanospheres and Their Corresponding Physical Parameters

samples	crystallite size (nm) ± 0.2 nm	BET surface area (m^2 g^{-1}) ± 5 m^2g^{-1}	UV exposure time (min)	MO degradation (%)
S-A	2.9	160	30	84
S-150	3.2	146	30	100
S-200		130	30	87
S-300	4.6	103	30	62
S-500	5.9	75	30	42

5.2. Gas Sensing Studies. SnO_2 is the material that has been widely studied for gas sensing application. Gas sensing being a surface active phenomenon, by adopting the procedure described above for the synthesis of porous nanospheres the improvement in the sensing performance can be effectively demonstrated. Gas sensing studies were performed systematically first to bring out the influence of porosity, increased surface area, and finally the role of additive in imparting selectivity.

The gas sensing studies involved measuring the sensor resistance at different operating temperatures, with different gas concentrations (1% up to 10 ppm H_2 in N_2) and response characteristics that give the sensor response as a function of time. The gas flow during these studies is maintained at 100 sccm. The sensor response (S) is defined as the change of electrical resistance of the material in the test gas normalized to the value of resistance in air $S = (R_a - R_g)/R_a$, where R_a is resistance in air and R_g is resistance in test gas.[21] The complete sensor characteristics comprise the response as a function of operating temperature, concentration of the test gas in air and the response as a function of time viz. response time and recovery time.

Figure 12a is the response of the sensor element of SnO_2 nanospheres as a function of operating temperature. It is seen that the sensor reaches saturation at about 180 °C. The basis for our claim of superior sensor response is the improved sensitivity at lower operating temperatures and quantifiable sensitivity even for very low concentrations of test gas in air. Our results are better than existing reports like the very recent work by H. Zhang et al on nanofibers,[33] where they reported sensitivity at higher operating temperatures for pure and Pd/SnO_2 and earlier work by B. Wang et al where they provided detailed comparative studies of SnO_2 sensor performance for H_2 gas with different morphologies.[34] Further, to demonstrate the performance of this SnO_2 as a selective hydrogen sensor, the porous SnO_2 nanospheres were surface modified with Pd. Figure 12b is the response of 0.5 wt % Pd/SnO_2 to hydrogen, which shows a drastic decrease in the operating temperature, and the sensor responds to hydrogen even at room temperature. This room temperature hydrogen sensing holds a lot of technological importance. From Figure 12c, it is evident that at corresponding operating temperatures, pure SnO_2 and Pd/SnO_2 show reasonable sensitivity even toward 50 ppm hydrogen gas. Lastly, Figure 12d shows the comparative response characteristics of SnO_2 and Pd/SnO_2 porous nanospheres. For both SnO_2 at an operating temperature of 180 °C and Pd/SnO_2 at an operating temperature of 50 °C the response times are less than 10 s and recovery times are nearly 20 s. Figure.13 is the cross sensitivity studies on 0.5 wt % Pd/SnO_2, which shows that at low temperatures, the material is selectively sensitive to hydrogen compared to the interfering gases such as ethanol, acetone and ammonia. As seen at higher temperatures the sensitivity to the interfering gases increases as expected. It is worth mentioning that these results even surpass our earlier reports on mesoporous Pd/SnO_2.[21] The present work evidently shows that the low-temperature gas sensing characteristics of SnO_2 porous nano spheres are notably enhanced by Pd incorporation. Consequently, the enhanced sensor properties are considered to result both from the unique porous structure of SnO_2 nanospheres and the catalytic effect of Pd nanoparticles. Physically, the porous SnO_2 nanospheres composed of numerous SnO_2 nanoparticles have a rough, loose and porous structure in comparison to the conventional tightly compacted particle films and closed hollow spheres.[15] This morphology favors the diffusion and transport of gas analyte and thereby shows a better sensor response.

6. CONCLUSIONS

In summary, a "Green synthetic methodology" has been demonstrated to obtain well-defined porous SnO_2 nanospheres at low temperature, i.e., 50 °C, without using any harmful or hazardous chemicals. Monodispersed and uniform-sized porous nanospheres of ~50 nm are formed with small SnO_2 nanocrystals of 2−3 nm with high surface area and the method is facile and easily up-scalable. This material shows significant photocatalytic response toward the degradation of methyl orange (MO), an organic pollutant. MO is degraded completely in 30 min with S-150 nanophotocatalyst and the material could be used repeatedly with the enhanced efficiency at least 5 times. The material also exhibits excellent gas sensing capabilities. Incorporation of 0.5 wt % Pd into SnO_2 matrix enhances the sensitivity and makes it highly selective for low temperature hydrogen detection. The material is able to respond to even 50 ppm H_2 in N_2 at room temperature with a response time of 10 s. These sensing properties are attributed

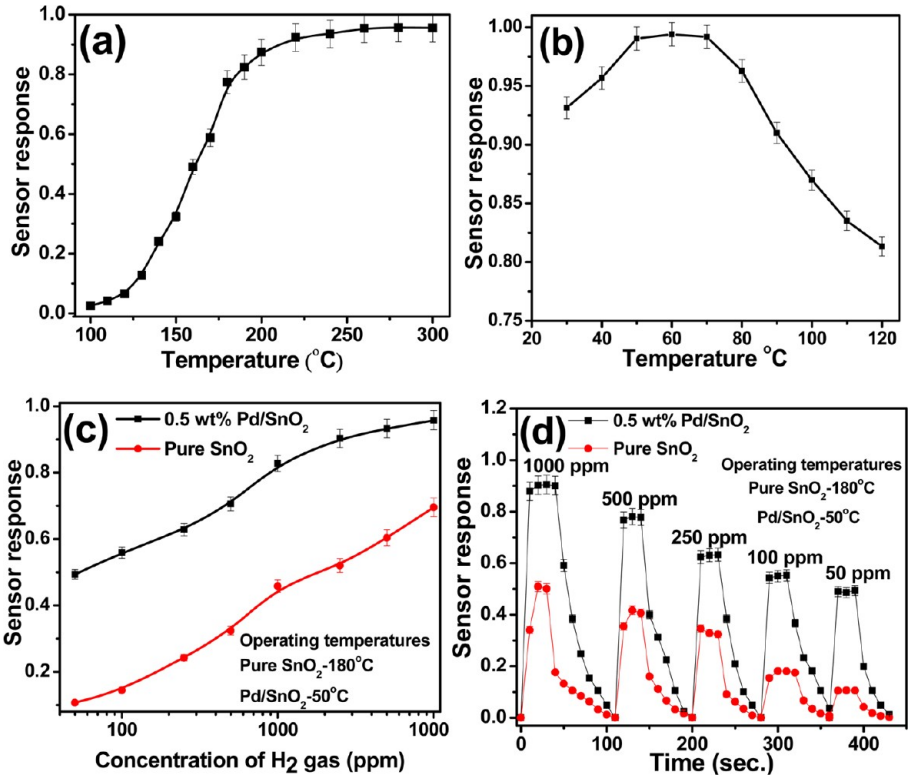

Figure 12. Gas sensing performance of SnO_2 nanospheres. (a) Sensor response of pure SnO_2 at different temperatures toward 1% hydrogen gas. (b) Sensor response of 0.5 wt % Pd/SnO_2 at various temperatures toward 1% hydrogen gas. (c) Sensor response of pure SnO_2 and Pd/SnO_2 at various hydrogen gas concentrations at corresponding operating temperatures. (d) Sensor response of pure SnO_2 and Pd/SnO_2 as a function of time at corresponding operating temperatures. The sensor operating temperatures for pure SnO_2 and Pd/SnO_2 are 180 and 50 °C, respectively.

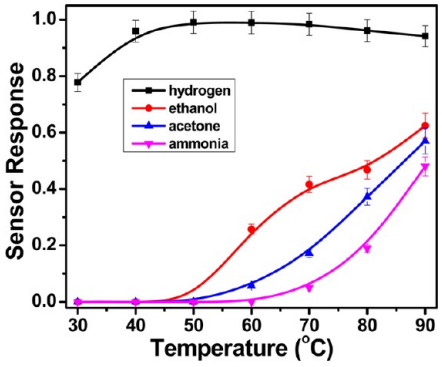

Figure 13. Sensor response versus temperature for 0.5 wt % Pd/SnO_2 toward different gases of 1% gas concentration.

to the synergism provided by the unique porous structure of SnO_2 nanospheres and the catalytic activity of the Pd nanoparticles.

■ ASSOCIATED CONTENT

Supporting Information

Experimental details, analyses by TEM, TG-DTA, FT-IR, EDX. and UV–vis absorption spectra for the photocatalytic studies on the porous SnO_2 nanospheres are provided. This material is available free of charge via the Internet at http://pubs.acs.org/.

■ AUTHOR INFORMATION

Corresponding Author

*E-mail: manorama@iict.res.in. Tel.: +91 40 27193225. Fax: +91 40 27160921.

Notes

The authors declare no competing financial interest.

■ ACKNOWLEDGMENTS

The DBT sponsored project GAP-0209 and DST-UK, APEX projects are gratefully acknowledged for the financial assistance. P.M. and B.R.R. acknowledge the CSIR and UGC respectively for the senior research fellowships.

■ REFERENCES

(1) Yang, H. G.; Zeng, H. C. *Angew. Chem., Int. Ed.* **2004**, *43*, 5930–5933.
(2) Kemp, G. L.; Marritt, S. J.; Xiaoe, L.; Durrant, J. R.; Cheesman, M. R.; Butt, J. N. *Biochem. Soc. Trans.* **2009**, *37*, 368–372.
(3) Cakan, R. D.; Hu, Y. S.; Antonietti, M.; Maier, J.; Titirici, M. M. *Chem. Mater.* **2008**, *20*, 1227–1229.
(4) Han, Y.; Wu, X.; Ma, Y.; Gong, L.; Qua, F.; Fan, H. *Cryst. Eng. Comm.* **2011**, *13*, 3506–3510.
(5) Wu, W.; Zhang, S.; Juan, Z.; Xiao, X.; Ren, F.; Jiang, C. *Chem.—Eur. J.* **2011**, *17*, 9708–9719.
(6) Shin, Y.; Bae, I. T.; Exarhos, G. J. *Colloids Surf., A* **2009**, *348*, 191–195.
(7) Tong, G.; Guan, J.; Zhang, Q. *Mater. Chem. Phys.* **2011**, *127*, 371–378.
(8) Li, C. C.; Yin, X. M.; Li, Q. H.; Wang, T. H. *Cryst. Eng. Comm.* **2011**, *13*, 1557–1563.
(9) Miao, Z.; Wu, Y.; Zhang, X.; Liu, Z.; Han, B.; Dinga, K.; Ana, G. *J. Mater. Chem.* **2007**, *17*, 1791–1796.
(10) Tatsuda, N.; Nakamura, T.; Yamamoto, D.; Yamazaki, T.; Shimada, T.; Inoue, H.; Yano, K. *Chem. Mater.* **2009**, *21*, 5252–5257.
(11) Chen, Y.; Chen, H.; Zeng, D.; Tian, Y.; Chen, F.; Feng, J.; Shi, J. *ACS Nano* **2010**, *4*, 6001–6013.

(12) Guo, Z. P.; Du, G. D.; Nuli, Y.; Hassanb, M. F.; Liub, H. K. *J. Mater. Chem.* **2009**, *19*, 3253−3257.
(13) Liu, J.; Luo, T.; Mouli, T. S.; Meng, F.; Sun, B.; Li, M.; Liu, J. *Chem. Commun.* **2010**, *46*, 472−474.
(14) Manjula, P.; Arunkumar, S.; Manorama, S. V. *Sens. Actuators, B* **2011**, *152*, 168−175.
(15) Zhang, J.; Liu, X.; Wu, S.; Xu, M.; Guo, X.; Wang, S. *J. Mater. Chem.* **2010**, *20*, 6453−6459.
(16) Huang, J. Y.; Zhong, L.; Wang, C. M.; Sullivan, J. P.; Xu, W.; Zhang, L. Q.; Mao, S. X.; Hudak, N. S.; Liu, X. H.; Subramanian, A.; Fan, H.; Qi, L.; Kushima, A.; Li, J. *Science* **2010**, *330*, 1515−1520.
(17) Park, M. S.; Wang, G. X.; Kang, Y. M.; Wexler, D.; Dou, S. X.; Liu, H. K. *Angew. Chem., Int. Ed.* **2007**, *46*, 750−753.
(18) Zhao, Q.; Gao, Y.; Bai, X.; Wu, C.; Xie, Y. *Eur. J. Inorg. Chem.* **2006**, 1643−1648.
(19) Wang, C.; Zhou, Y.; Ge, M.; Xu, X.; Zhang, Z.; Jiang, J. Z. *J. Am. Chem. Soc.* **2010**, *132*, 46−47.
(20) Wu, S.; Cao, H.; Yin, S.; Liu, X.; Zhang, X. *J. Phys. Chem. C* **2009**, *113*, 17893−17898.
(21) Manjula, P.; Satyanarayana, L.; Swarnalatha, Y.; Manorama, S. V. *Sens. Actuators, B* **2009**, *138*, 28−34.
(22) Han, X.; Jin, M.; Xie, S.; Kuang, Q.; Jiang, Z.; Jiang, Y.; Xie, Z.; Zheng, L. *Angew. Chem., Int. Ed.* **2009**, *48*, 9180−9183.
(23) Yeow, S. C.; Ong, W. L.; Wong, A. S. W.; Ho, G. W. *Sens. Actuators, B* **2009**, *143*, 295−301.
(24) Burgard, D.; Goebbert, C.; Nass, R. D. *J. Sol−Gel Sci. Technol.* **1998**, *13*, 789−792.
(25) Ning, J.; Dai, Q.; Jiang, T.; Men, K.; Liu, D.; Xiao, N.; Li, C.; Li, D.; Liu, B.; Zou, B.; Zou, G.; Yu, W. W. *Langmuir* **2009**, *25*, 1818−1821.
(26) Lou, X. W.; Wang, Y.; Yuan, C.; Lee, Y.; Archer, J. L. A. *Adv. Mater.* **2006**, *18*, 2325−2329.
(27) Yang, S.; Gao, L. *J. Am. Ceram. Soc.* **2006**, *89*, 1742−1744.
(28) Popescu, D. A. M.; Verduraz, F. B. O. *Catal. Today* **2001**, *70*, 139−154.
(29) Gyger, F.; Hubner, M.; Feldmann, C.; Barsan, N.; Weimar, U. *Chem. Mater.* **2010**, *22*, 4821−4827.
(30) Ho, S. Y.; Wong, A. S. W.; Ho, G. W. *Cryst. Growth Des.* **2009**, *9*, 732−736.
(31) Penn, R. L.; Banfield, J. F. *Science* **1998**, *281*, 969−971.
(32) Tian, C.; Zhang, Q.; Wu, A.; Jiang, M.; Liang, Z.; Jiang, B.; Fu, H. *Chem. Commun.* **2012**, *48*, 2858−2860.
(33) Zhang, H.; Li, Z.; Liu, L.; Xu, X.; Wang, Z.; Wang, W.; Zheng, W.; Dong, B.; Wang, C. *Sens. Actuators, B* **2010**, *147*, 111−115.
(34) Wang, B.; Zhu, L. F.; Yang, Y. H.; Xu, N. S.; Yang, G. W. *J. Phys. Chem. C* **2008**, *112*, 6643−6647.